Journal of Alloys and Compounds 509 (2011) L208–L212

Contents lists available at ScienceDirect

Journal of Alloys and Compounds

journal homepage: www.elsevier.com/locate/jallcom

Letter

Enhanced ferroelectric, dielectric and optical behavior in Li-doped ZnO nanorods

Manoj K. Gupta, Binay Kumar*

Crystal Lab, Department of Physics & Astrophysics, University of Delhi, Delhi 7, India

ARTICLE INFO

Article history:
Received 6 October 2010
Received in revised form 16 March 2011
Accepted 19 March 2011
Available online 29 March 2011

Keywords:
Nanostructured materials
Ferroelectrics
Chemical synthesis
Dielectric response
Phase transitions
Optical spectroscopy

ABSTRACT

Enhancement in the dielectric and ferroelectric properties has been observed in case of Li-doped ZnO nanorods (NR). Effect of Li-doping on ZnO structure and its optical properties has also been reported. In high resolution TEM studies, the length and diameter of as-synthesized Li–ZnO nanorods were found in the range of 100–150 nm and 20–70 nm, respectively. XRD studies, Li-doped ZnO NR exhibited wurzite structure in which lattice parameter becomes larger than the pure ZnO NR. In dielectric studies, higher dielectric constant and a ferroelectric phase transition at 72 °C were observed. In ferroelectric studies, high remnant polarization of 0.873 μC/cm^2 and low coercive field of 0.592 kV/cm were observed, which were better than their values in bulk Li-doped ZnO (0.044 μC/cm^2 and 2.0 kV/cm, respectively). In UV–Vis spectra, low absorption band edge at 352 nm was observed due to the size effect in the ZnO nanorods. In addition, PL spectra show a blue shift in both UV and visible region as a result of doping. These results are discussed in the light of the nanorods of confined geometry.

© 2011 Elsevier B.V. All rights reserved.

1. Introduction

Quasi-one-dimensional 1D ZnO nanostructures such as nanowires and nanorods have received tremendous attention in the last decade, because they exhibit different and controllable physical properties than their bulk counterpart. The effect of broad range of properties of ferroelectric nanostructure, such as high transition temperature, spontaneous polarization, remnant polarization, dielectric permittivity as well as piezo- and pyro-electricity, make ferroelectric nanorods/nanowires an extremely interesting material class for research as well as for applications. Zinc oxide (ZnO) is a wide direct band gap semiconductor of (E_g) 3.37 eV that displays unique features such as large exciton binding energy (E_b) 60 meV and large piezoelectric and ferromagnetic coefficients with a predicted curie temperature above room temperature when doped with transition metals [1,2]. Doped zinc oxide (ZnO) nanostructures are studied extensively because of their application to ferroelectric memories, nanosensors, SAW devices, nanogenerator, and nano-optoelectronics devices [3–6]. Since ZnO can be synthesized in both p-and n-type structure, ZnO NR assume much importance for various p–n junction based electronic and optoelectronic nano-devices [7,8]. Various methods have been developed to synthesize nano-structure ZnO, such as reaction-vapor deposition [9], physical vapor deposition [10], metal organic chemical vapor deposition (MOCVD) and hydrothermal method [11,12]. Recently, wet chemical methods have been proved to be very suitable for the synthesis of low-dimensional ZnO nanostructures with high uniformity [13,14].

In this context, the ferroelectricity of properly synthesized Li-doped Zinc oxide (ZnO) nanorods has become an interesting topic. We used a low-temperature wet chemical approach for the preparation of straight Li-doped ZnO nanorods. The structural, morphological, optical, dielectric and ferroelectric properties of the samples were studied. The effect of Li metal intercalation on the electronic, optics, and field emission properties is a subject under study for several research groups [15,16]. Ferroelectric behavior was found in bulk Li-doped ZnO although no phase transition had been reported in pure ZnO at atmospheric pressure [17–22]. Further, till now there is no report of dielectric and ferroelectric study of Li-doped ZnO nanorods. We demonstrate here the enhanced dielectric constant, remnant polarization and reduced coercive field of Li-doped ZnO which enable its use in the field of nano-storage and nano-memories devices. In addition, the dielectric properties and optical properties (high dielectric constant, low cutoff in UV–Vis) are also promoted their storage and optical applications.

2. Experimental details

Li-doped ZnO nanorods were synthesized by wet chemical solution route. In this process, zinc chloride and sodium hydroxide were taken in the molar ratio of 1:7 and dissolved into water. Sodium hydroxide solution was mixed homogeneously into $ZnCl_2$ aqueous solution, stirred at room temperature for 30 min. 0.2 M $LiCO_3$ was added slowly and the whole solution was again stirred at room temperature for 2 h. After homogenization, the solution was kept in a constant temperature oil bath for 3 h at 90 °C. The sample was washed by distilled water and ethanol several times. Finally, brownish powder was obtained by centrifugation. The as-grown samples were characterized by X-ray diffraction (XRD) with a Bruker D8 Advance Cu

* Corresponding author. Tel.: +91 9818168001; fax: +91 011 27667061.
E-mail address: bkumar@physics.du.ac.in (B. Kumar).

0925-8388/$ – see front matter © 2011 Elsevier B.V. All rights reserved.
doi:10.1016/j.jallcom.2011.03.119

$K\alpha_1$, $\lambda = 1.5405$ Å at room temperature. The formation of nanorods was confirmed by high-resolution transmission electron microscopy (HRTEM) which was carried out by a Tecnai 300 kV Ultra twin (FEI Company) with an attached energy-dispersive X-ray spectrometer (EDS). TEM samples were prepared by dispersing the powder in ethanol by ultrasonic treatment, positioning a drop onto a porous carbon film supported on a copper grid, and then drying it in air. UV–Vis absorption spectrum was performed by Perkin Elmer UV Win Lab spectrometer. The room-temperature photoluminescence (PL) measurements were carried out on a Fluorolog-3 spectrometer (Jobin Yvon Co. Ltd.) using a Xe lamp as the excitation source. The dielectric constant of ZnO nanorods was measured using an Agilent E 4980A LCR meter for a frequency range 1 kHz to 2 MHz in the temperature range of 20–150 °C. Ferroelectric hysteresis was measured using an indigenously built Sawyer–Tower circuit driven by a lock-in amplifier.

3. Results and discussion

The phase of the as-grown samples and their crystallographic orientation were identified by XRD measurement. Fig. 1 depicts the XRD patterns of the as grown Li-doped ZnO nanorods at room temperature. XRD peaks implying the formation of wurzite structure of Li-doped ZnO. The grain sizes of the ZnO nanorods calculated from the Scherrer's formula were found to be 34, 43 and 31 nm along (1 0 0), (0 0 2) and (1 0 1) planes, respectively. It clearly shows that the grain size along crystalline plane (0 0 2) is high, which is an indication of preferentially anisotropic growth of ZnO nanorods along the [0 0 0 1] direction (the *c* axis).

The lattice parameter of Li-doped ZnO nanorods are found to be $a = 3.2555$ Å and $c = 5.210$ Å at room temperature by using PowderX and Check Cell Software. The reported values for pure ZnO are $a = 3.249858$ Å and $c = 5.206619$ Å (JCPDS 36-1451). The lattice parameters were found to be slightly larger in Li-doped ZnO. The increase in the lattice parameter must be caused by either interstitial incorporation of Li^+ into the lattice or the formation of electrically inactive Li_{Zn}–Li_i pairs [23]. The ratio a/c of Li doped ZnO nanorods is 0.62486, which is slightly larger than that of pure ZnO (0.62418). This value is related to the positional parameter u in the structure by

$$u = \frac{a^2}{3c^2} + 0.25 \quad (1)$$

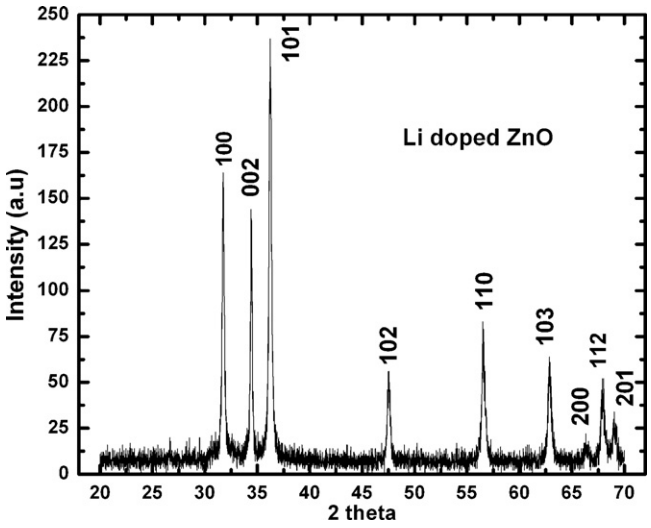

Fig. 1. XRD pattern of Li doped ZnO nanorods.

and the Zn–O bond length l is given by

$$l = \sqrt{\frac{a^2}{3} + \left(\frac{1}{2} - u\right)^2 c^2} \quad (2)$$

The calculated value of Zn–O bond in doped case is 1.988 Å which is slightly more than 1.9778 Å for undoped ZnO [24]. This small structural distortion may drive the ferroelectric phase transition.

Fig. 2a shows the HR-TEM image of the pure ZnO nanorods. The diameter and length of the nanorods is found to be ~30 nm and ~300 nm, respectively. In the case of the as-prepared Li-doped ZnO, the length of the nanorods has been reduced to 100–120 nm while the diameter remains nearly unchanged (Fig. 2b). A narrow size distribution and shape uniformity can be seen in both pure and doped ZnO NR. Further, there are no indications of secondary phases in the (HR)TEM pictures, suggesting that all dopant atoms are homo-

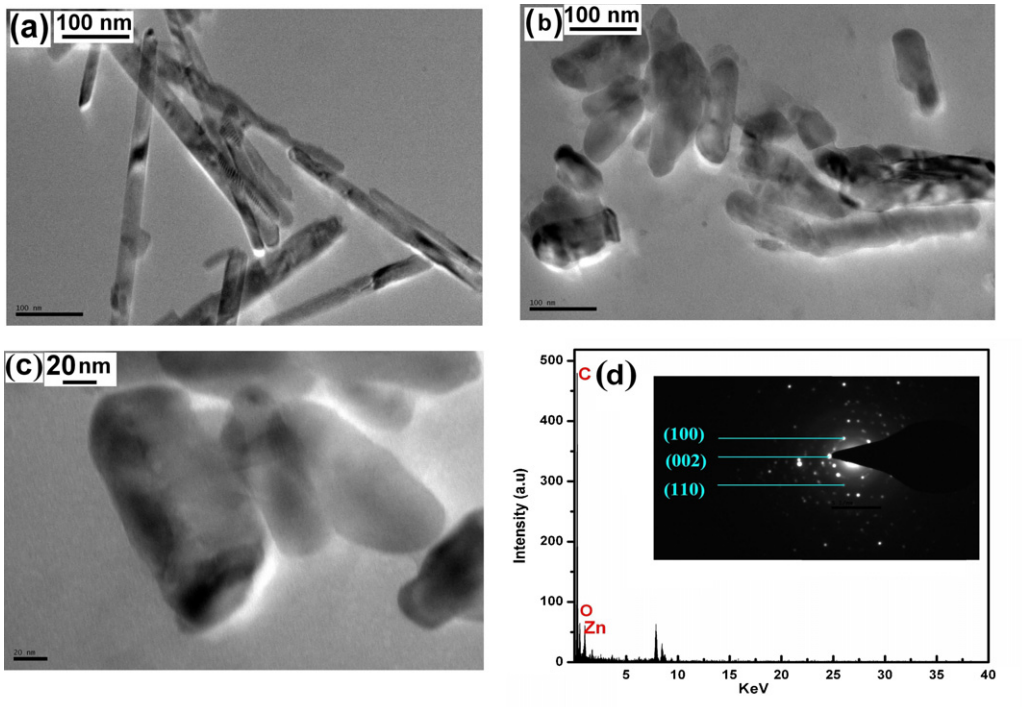

Fig. 2. (a) HRTEM image of pure ZnO; (b) and (c) HRTEM image of Li-doped ZnO nanorods; (d) EDS and SAED (inset) spectrum of Li-doped ZnO.

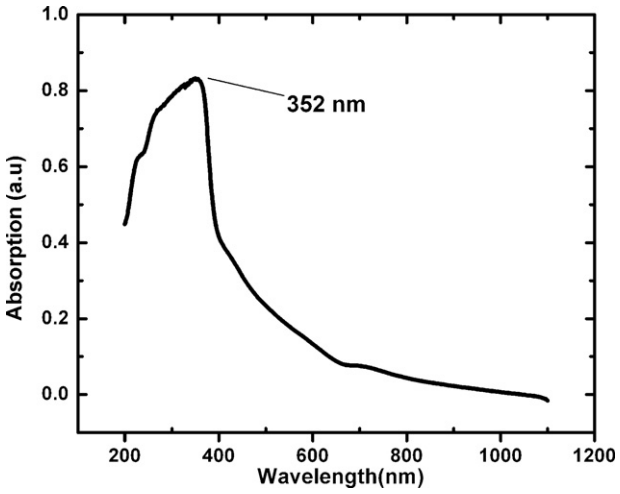

Fig. 3. UV spectrum of Li-doped ZnO indicating a blue shift.

geneously incorporated into the ZnO rods and that no Li clustering occurred, even in higher magnification (Fig. 2c). Further, a reduced surface area for doped nanorods is clearly visible.

In EDS spectra (Fig. 2d), only oxygen and zinc signals were observed for nanorods within the limit of the EDS measurement because Li cannot be detected by the EDS due to its low atomic number. However, it is an indication that ZnO:Li nanorods do not contain secondary phases and that the incorporation of the Li in the ZnO structure is at atomic level. In the inset of Fig. 2d, the selected area electron diffraction (SAED) pattern shows that the single-crystalline Li–ZnO nanorods are uniformly grown along [0 0 1] growth direction.

Fig. 3 depicts a UV–Vis spectrum of the as-prepared Li–ZnO nanorods, which was obtained on a Perkin Elmer UV Win Lab spectrometer. In UV–Vis absorption spectra, a sharp absorption band-edge around 352 nm is observed which is in good agreement with the reported value of ZnO nanorods. The absorbance edge for pure bulk ZnO is reported at a wavelength of 375 nm [25]. The observed blue shift of 23 nm in the Li-doped ZnO nanorods as compared to bulk crystal may be due to the quantum confinement effect from the small individual crystal size, making these nanocrystals more suitable for UV applications.

PL spectrum of the Li-doped ZnO nanorod is shown in Fig. 4a. In general, the room temperature PL spectra of as-grown ZnO and Li doped ZnO revealed a clear shift of emission band in visible region with intensity. However, in ultraviolet region, the emission were found to be little shifted i.e. 378 nm for Li-doped and 381 nm for pure ZnO (Fig. 4b). There appeared weak emission bands at about 381 nm which comes from the recombination of free excitons [26] and is generally assigned as a near-band-edge (NBE) emission band. Another strong broad band emission with higher intensity at wavelength 565 nm for Li doped ZnO and 581 nm (green emission) for pure ZnO were observed. The shifts in emission position from 581 to 565 nm show the effect of Li doping into ZnO structure. The green emission in ZnO results from the recombination of a photogenerated hole with a singly ionized oxygen vacancy [26]. The blue shift is due to shift in UV absorption cut off as shown in Fig. 3 and which is due to the Burstein–Moss effect resulting from Li doping in ZnO nanorods. ZnO is well known as an n-type semiconductor, and when it is doped, Li will contribute electrons to the conduction band to such an extent that the Fermi level of ZnO will move inside the conduction band by the quantity ξn. Since the states below ξn of the conduction band are filled, the absorption edge should shift towards the higher energy by ξn (towards lower wavelength side)

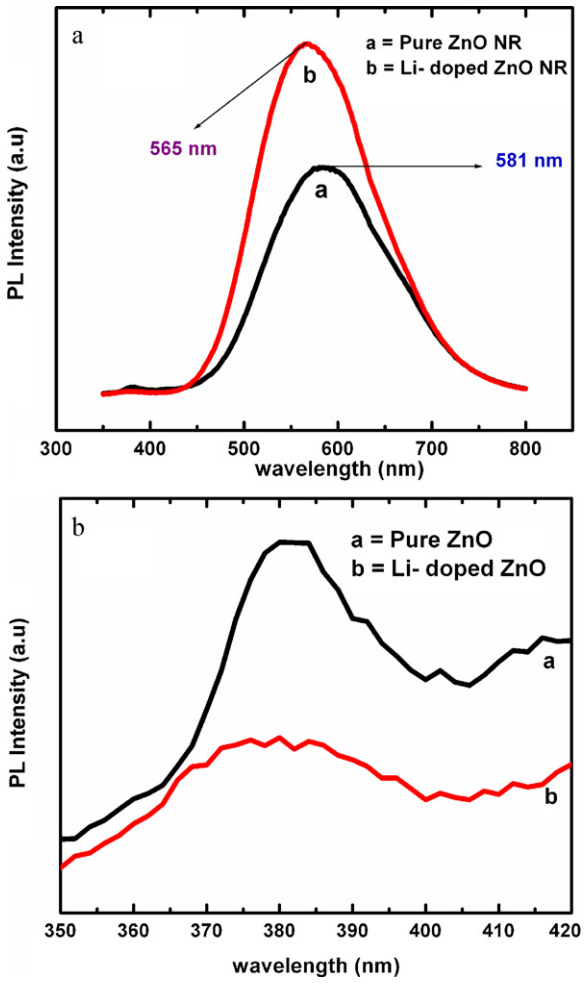

Fig. 4. (a) Photoluminescence of Li-doped ZnO nanorods at excitation wavelength at. 325 nm. (b) Close-up of near band emission of Li-doped ZnO.

[27].

It is observed that the dielectric constant (ε) of Li-doped ZnO nanorods decreases with increase in frequency Fig. 5a. At room temperature, the dielectric constant at lower frequency region at 1 kHz at RT is high ($\varepsilon \sim 19$) for Li-doped ZnO nanorods as compared to bulk Li-doped ZnO ($\varepsilon \sim 9$) [28]. The dielectric loss ($\tan\delta$) decreases with increase in frequency and dielectric loss of Li-doped ZnO nanorods is 0.03 at 2 MHz at RT (Fig. 5b).

The observed large value of dielectric constant is due to the fact that the nanocrystals of ZnO under the application of electric field act as nanodipoles. As the particle size is small, the number of particles per unit volume is very large resulting in an increase in the dipole moment per unit volume and hence the high dielectric constant [29]. Dielectric constant and dielectric loss with variations of temperatures at different frequencies for Li–ZnO nanorods are shown in Fig. 5c and d. It is observed that the dielectric constant (ε) increases with increase in temperature up to 72 °C and then it start decreasing. Similar behavior was also found in dielectric loss ($\tan\delta$). This suggests a ferroelectric to paraelectric phase transition in Li-doped ZnO nanorods which is being reported for the first time. This ferroelectric phase transition in ZnO nanorods is due to the structural modifications induced by Li dopant in ZnO, which greatly affect the electronic and dielectric properties, leading to the appearance of ferroelectricity. In this case T_c was observed at 72 °C which is much higher than that observed for bulk Li-doped ZnO in different reports (Table 1). Thus in the present case, a wider temperature range for ferroelectric phase is obtained. In nanorods

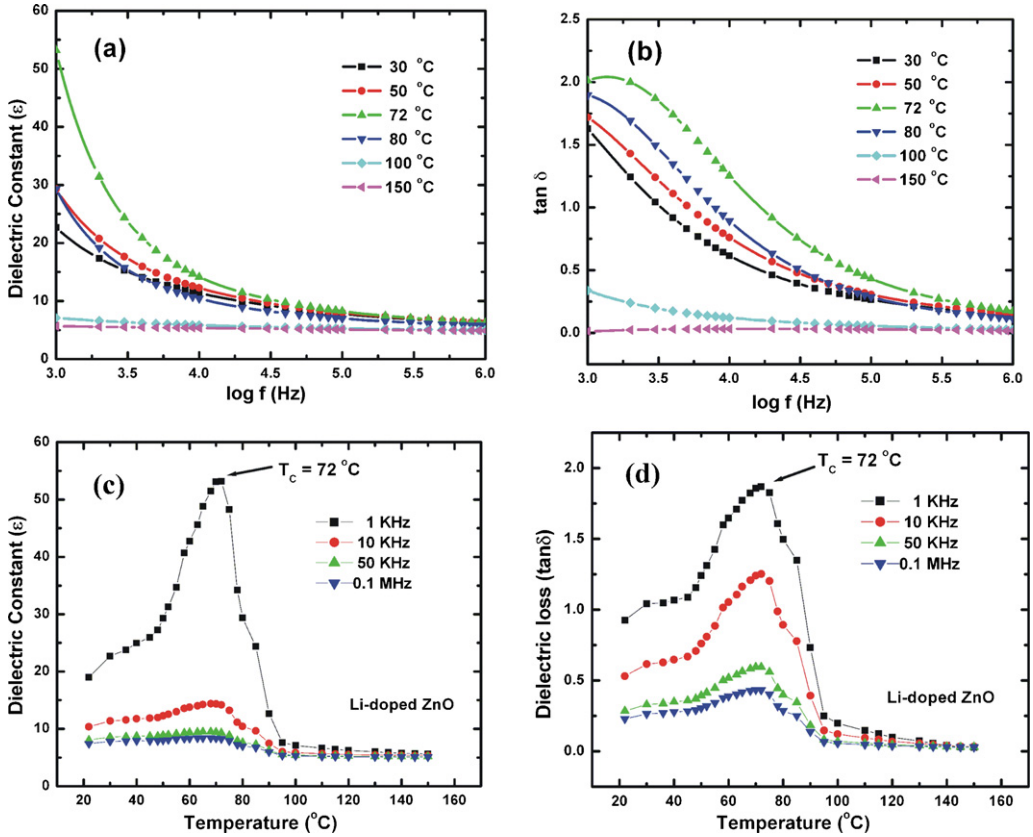

Fig. 5. (a) Variation of dielectric constant vs. applied frequency. (b) Variation of dielectric loss vs. applied frequency. (c) Variation of dielectric constant vs. temperature. (d) Variation of dielectric loss vs. temperature.

structure, the surface pressure $P \sim \mu/R$ can increase the transition temperature via electrostriction effect which correlate the formula given by Morozovska et al. [31].

$$T_c^* = T_c - 2Q_{12}\frac{\mu}{\alpha_T R} \quad (3)$$

where T_c^* is Curie temperature of nanorods, T_c is Curie temperature of bulk, Q_{12} is electrostriction parameter, μ is the effective surface coefficient, α_T is proportional to inverse of Curie constant and R is the radius of nanorods. For bulk materials $R \to \infty$ and therefore $T_c^* = T_c$ i.e. no change of transition temperature. For Li:ZnO nanorods, $R \approx 20$ nm and $Q_{12} < 0$ for hexagonal system [32] which results in $T_c^* > T_c$ form above equation. It explains the increased transition temperature in Li–ZnO as compared to bulk ZnO. In addition, the radial pressure, caused by the surface tension in Li:ZnO NR, is responsible for enhanced ferroelectricity in the present case.

Finally, the polarization (P–E) curve was traced using a standard computer controlled Sawyer–Tower hysteresis bridge at room temperature by applying an external voltage up to 5 kV/cm (Fig. 6). The remnant polarization (P_r) and the coercive field (E_c) of the sample were found to be 0.873 μC/cm^2 and 0.59 kV/cm, respectively. Higher field was not applied to avoid sample damage. The values of P_r and E_c for bulk Li-doped ZnO are given in Table 1. It is evident that the P_r value for NR is much higher than for the bulk Li–ZnO. The high value of remnant polarization (P_r) and low value of coercive field (E_c) in Li-doped ZnO nanorods highlight its importance in nanoscale nonvolatile ferroelectric memories devices. The origin of this ferroelectric behavior could be explained on the basis of the ionic radii difference between the Zn^{2+} (0.74 Å) and the dopant ions

Table 1
Comparison of ferroelectric parameters of bulk and Li-doped ZnO nanorods.

Li-doped ZnO	Curie temperature (°C)	P_r (μC/cm^2)	E_c (kV/cm)	Reference
Li-doped ZnO	68	0.21	5.86	[21]
$Zn_{0.9}Li_{0.1}O$	57	0.044	2.0	[17]
$Zn_{0.9}Li_{0.1}O$	57	0.051	2.7	[19]
Li-doped ZnO film	67	0.193	4.8	[30]
Li-doped ZnO nanorods	72	0.873	0.59	[Present work]

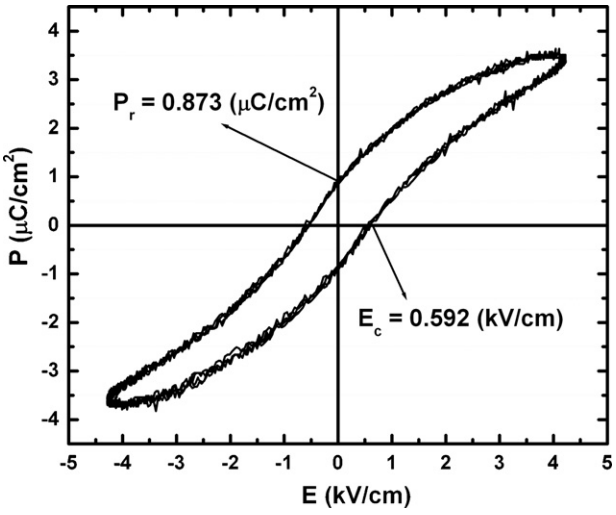

Fig. 6. Ferroelectric hysteresis loop of Li-doped ZnO nanorods.

Li^+ (0.60 Å). Due to this ionic size difference, Li^+ ions can occupy the off-centered positions, which lead to permanent local electric dipoles and thereby induce ferroelectric behavior [17–19]. This room temperature ferroelectric property in nanorods of Li-doped ZnO is significant because the suspected possible disappearance of ferroelectricity nature at a finite critical volume was not encountered till a radius of ~20 nm in the present case. In addition, the increase of P_r is also adding a strong support for those results in which the noticeable enhancement of ferroelectric properties appears in nanostructures [33,34].

4. Conclusions

In conclusion, synthesis of ferroelectric Li doped ZnO nanorods by wet chemical route and enhancement of various ferroelectric and optical properties due to Li-incorporation in ZnO NR are reported. The Zn–O bond length are calculated and found to be 1.988 Å. UV measurements show increase in optical band gap due to nanocrystalline nature. The blue shift in PL spectra shows a strong effect of Li into ZnO lattice. In dielectric characterization of Li doped ZnO NR, a ferroelectric phase transition was observed at a higher temperature of 72 °C. Li incorporation in ZnO NR resulted in higher dielectric constant (19), higher remnant polarization and lower coercive field as compared to bulk Li–ZnO. This wide ferroelectric region (high transition temperature) and enhanced ferroelectric parameters play an important role in the miniaturization of devices and make Li-doped ZnO a promising candidate for nano-optoelectronics, nanostorage and nanoscale memory devices.

Acknowledgements

We are thankful for the financial support from the Department of Science and Technology, India under SERC project (Sanction No. 100/IFD/1637). Mr. M.K. Gupta is thankful to DST for Senior Research Fellowship.

References

[1] T. Diet, H. Ohno, F. Matsukura, J. Cibert, D. Ferrand, Science 287 (2000) 1019.
[2] R. Janisch, P. Gopal, N.A. Spaldin, J. Phys.: Condens. Mat. 17 (2005) R657.
[3] M. Dawber, K.M. Rabe, J.F. Scott, Rev. Mod. Phys. 77 (2005) 1083.
[4] X. Wang, C.J. Summers, Z.L. Wang, Nano Lett. 43 (2004) 423.
[5] T. Yamamoto, T. Shiosaki, A. Kawabata, J. Appl. Phys. 51 (1980) 3113.
[6] Z.L. Wang, J. Song, Science 31 (2006) 2242.
[7] M. Sun, Q.F. Zhang, W.J. Lei, J. Phys. D: Appl. Phys. 40 (2007) 3798.
[8] M.K. Gupta, N. Sinha, B.K. Singh, B. Kumar, Mater. Lett. 64 (2010) 1825.
[9] H.Z. Zhang, X.C. Sun, R.M. Wang, D.P. Yu, J. Cryst. Growth 269 (2004) 464.
[10] Y.C. Kong, D.P. Yu, B. Fang, S.Q. Feng, Appl. Phys. Lett. 78 (2001) 407.
[11] H.W. Kim, N.H. Kim, J.H. Shim, N.H. Cho, C. Lee, J. Mater. Sci.: Mater. Electron. 16 (2005) 13.
[12] B. Liu, H. Zeng, J. Am. Chem. Soc. 125 (2003) 4430.
[13] L. Guo, Y. Ji, H. Xu, J. Am. Chem. Soc. 124 (2002) 14864.
[14] M.K. Gupta, N. Sinha, B.K. Singh, N. Singh, K. Kumar, B. Kumar, Mater. Lett. 63 (2009) 1910.
[15] D. Uki, H. Ohnishi, T. Yamaguchi, Y. Takemori, A. Koizumi, S. Fuchi, T. Ujihara, Y. Takeda, J. Cryst. Growth 298 (2007) 69.
[16] N.R. Aghamalyan, R.K. Hovsepyan, S.I. Petrosyan, J. Contemp. Phys. 43 (2008) 177.
[17] A. Onodera, N. Tamaki, Y. Kawamura, T. Sawada, H. Yamashita, Jpn. J. Appl. Phys. 35 (1996) 5160.
[18] A. Onodera, N. Tamaki, K. Jin, H. Yamashita, Jpn. J. Appl. Phys. 36 (1997) 6008.
[19] N. Tamaki, A. Onodera, T. Sawada, H. Yamashita, J. Kor. Phys. 29 (1996) S668.
[20] A. Onodera, N. Tamaki, Y. Kawamura, T. Sawada, N. Sakagami, K. Jin, H. Satoh, H. Yamashita, J. Kor. Phys. 32 (1998) S11.
[21] Z.C. Wu, X.M. Zhang, J.M. Liu, Q.C. Li, X.Y. Chen, J. Yin, N. Xu, Z.G. Liu, Ferroelectrics 252 (2001) 265.
[22] X.S. Wang, Z.C. Wu, J.F. Webb, Z.G. Liu, Appl. Phys. A77 (2003) 561.
[23] M.G. Wardle, J.P. Goss, P.R. Briddon, Phys. Rev. B 71 (2005) 155.
[24] J. Albertsson, S.C. Abrahams, A. Kvivk, Acta Crystallogr. B 45 (1989) 34.
[25] Y.C. Zhang, X. Wu, X.Y. Hu, R. Guo, J. Crystal Growth 280 (2005) 250.
[26] M.H. Huang, Y. Wu, H. Feick, N. Tran, E. Weber, P. Yang, Adv. Mater. 13 (**2**) (2001) 113.
[27] E. Burstein, Phys. Rev. 93 (1954) 632.
[28] A. Onodera, K. Yoshio, H. Satosh, H. Yamashita, T. Sawada, N. Sakagami, Jpn. J. Appl. Phys. 37 (1998) 5315.
[29] S. Bhattacharya, S.K. Saha, D. Chakravorty, Appl. Phys. Lett. 76 (2000) 389.
[30] C.W. Zou, M. Li, H.J. Wang, M.L. Yin, C.S. Liu, L.P. Guo, D.J. Fu, T.W. Kang, Nucl. Inst. Meth. Phys. Res. B 267 (2009) 1067.
[31] A.N. Morozovska, E.A. Elisev, M.D. Glinchuk, Phys. Rev. B 73 (2006) 214106.
[32] I. Kornev, M. Willatzen, B. Lassen, L.C.L.Y. Voon, AIP Conf. Proc. 1199 (2010) 71.
[33] D. Yadlovker, S. Berger, Phys. Rev. B 71 (2005) 184112.
[34] G. Geneste, E. Bousquest, J. Junquera, P. Chosez, Appl. Phys. Lett. 88 (2006) 112906.